# Structures and Energetics for $O_2$ Formation in Photosystem II

PER E. M. SIEGBAHN

*Department of Physics, ALBA NOVA, and Department of Biochemistry and Biophysics, Arrhenius Laboratory, Stockholm University, SE-106 91 Stockholm, Sweden*
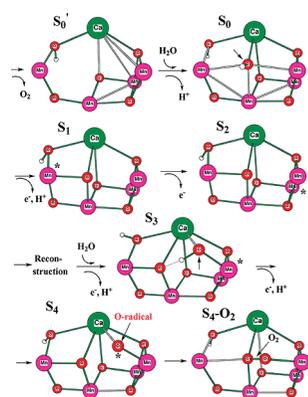
RECEIVED ON JUNE 19, 2009

## CONSPECTUS

Water oxidation, forming $O_2$ from water and sunlight, is a fundamental process for life on earth. In nature, the enzyme photosystem II (PSII) catalyzes this reaction. The oxygen evolving complex (OEC), the complex within PSII that catalyzes the actual formation of the O−O bond, contains four manganese atoms and one calcium atom connected by oxo bonds. Seven amino acid side chains in the structure, mostly carboxylates, are ligated to the metal atoms. In the study of many enzyme mechanisms, theoretical modeling using density functional theory has served as an indispensable tool. This Account summarizes theoretical research to elucidate the mechanism for water oxidation in photosynthesis, including the most recent findings.



The development of successively larger models, ranging from 50 atoms in the active site up to the present model size of 170 atoms, has revealed the mechanism of $O_2$ formation with increasing detail. The X-ray crystal structures of PSII have provided a framework for optimizing the theoretical models. By constraint of the backbone atoms to be at the same positions as those in the X-ray structures, the theoretical structures are in good agreement with both the measured electron density and extended X-ray absorption fine structure (EXAFS) interpretations. By following the structural and energetic changes in those structures through the different steps in the catalytic process, we have modeled the oxidation of the catalytic complex, the binding of the two substrate water molecules, and the subsequent deprotonations of those substrate molecules.

In these models, the OEC forms a basin into which the water molecules naturally fit. These findings demonstrate that the binding of the second water molecule causes a reconstruction, results that are consistent with earlier EXAFS measurements. Most importantly, this Account describes a low-barrier mechanism for formation of the O−O bond, involving an oxygen radical that reacts with a $\mu$-oxo ligand of the OEC. Further research revealed that the oxygen radical is bound in the $Mn_3Ca$ cube rather than to the outside manganese. This Account provides detailed diagrams of the energetics of the different S-transitions both without and with a membrane gradient. An interesting detail of these reactions concerns the role of the tyrosine (Tyr$_Z$), which appears as an intermediate radical in the oxidation of the OEC. By simple electrostatic arguments, these results show that the initial oxidation of Tyr$_Z$ is downhill for the first two transitions but uphill for the final ones. In these later transitions, the oxidation of the OEC is coupled to deprotonations of water.

## I. Introduction

Light-driven hydrogen production from water by biomimetic methods is a promising approach to address the growing problems of the green-house effect and the energy crisis. In nature, photosystem II (PSII) is the only enzyme that can oxidize water with the help of sunlight. For this reason and since dioxygen formation from water is one of the most fundamental reactions for the evolution of life on earth, it has for decades been a high-priority scientific goal to understand this process. Until rather recently, experimental techniques were the only means to proceed. However, since water oxidation is a very complicated process involving a large number of transition states and at least a dozen intermediates, many of them

short-lived, it has now been realized that it is not possible to understand this process without detailed model calculations.

In this Account, the most recent efforts to understand water oxidation in PSII using the cluster model approach[1] will be described. After the event of the first X-ray structures of PSII,[2,3] realistic models of the active site could begin to be used. In previous reviews,[4−10] results for models with gradually increasing cluster size have been described. Many of the early findings have been confirmed in the later studies, like O−O bond formation involving an oxygen radical[11,12] and an endergonic formation of this radical,[13] but new findings have also completed the picture of the entire process. One of the major findings in a recent study was an origin for the reconstruction observed by extended X-ray absorption fine structure (EXAFS)[14,15] for the $S_2$ to $S_3$ transition. In this Account, a modification of this reconstruction, leading to a slightly different transition state for O−O bond formation, will be described. A new aspect is also that energy diagrams including $Tyr_Z$ oxidation by $P_{680}^+$ are given, as well as diagrams with and without a membrane gradient. Most results given here refer to models with about 170 atoms.

## II. Methods and Models

The density functional theory (DFT) calculations discussed here were made using the hybrid functional B3LYP*, which is a modification of the original B3LYP functional[16] with a reduction of the exact exchange to 15%.[17] Procedures used were very similar to those in previous studies,[8,9] with polarized basis sets for the geometries (lacvp*), large basis sets for energies (cc-pvtz(−f)), and a surrounding dielectric medium with dielectric constant equal to 6.0 (basis lacvp*). The performance of the B3LYP functional for the present type of problems has recently been reviewed,[18] indicating a typical accuracy within 3−5 kcal/mol, normally overestimating barriers. A different procedure than that used by other workers for obtaining redox potentials and $pK_a$ values is a key feature of the present approach.[4,6−9,13] Using experimental information about the driving force and a single adjustable parameter, one can determine accurate values for these properties without explicitly describing the enzyme surrounding the active site. The results are essentially independent of the choice of dielectric constant. The calculations were performed with the programs Jaguar[19] and Gaussian03.[20]

The chemical models used here are built on the X-ray structures,[2,3] schematically shown in Figure 1. These structures were obtained at a rather low resolution of 3.0−3.5 Å, and the exact ligation to the metal atoms therefore had to be
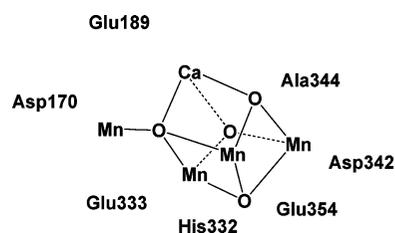


**FIGURE 1.** Simplified picture of the structure of the oxygen-evolving complex, suggested by X-ray crystallography.[2] In the more recent structure,[3] the manganese outside the cube is further out.
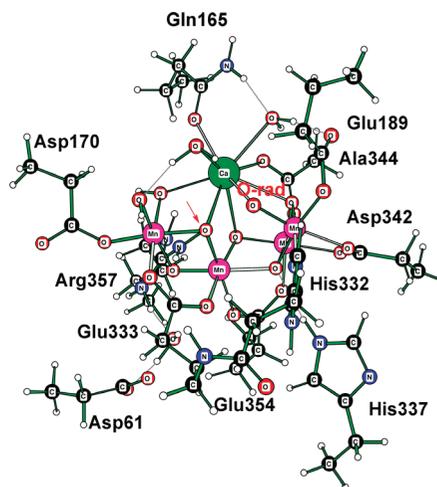


**FIGURE 2.** The model used for most of the results presented here, taken from a fully optimized structure of an $S_4$-state. The reacting oxygen radical is marked with O-rad, and an arrow marks the second oxygen.

partly assumed. In the London X-ray structure,[2] the binding of the carboxylate amino acid ligands (aspartates and glutamates) was assumed to be mostly monodentate to one metal. In contrast, in the Berlin X-ray structure,[3] most of these ligands were assumed to be bridging between two different metals. Possibilities between these two types of ligations are also possible. This means that a ligation pattern has to be assumed as a starting point for the computational model studies. In the more recent studies, a ligand pattern close to the one from the Berlin structure was adopted as being more chemically reasonable. It should be added that, in principle, the optimal ligation pattern could be obtained by direct minimization, but the possibilities are so many that this is in practice not possible.

A chemical model of the type used in most of the calculations discussed here is shown in Figure 2. Eleven amino acids were included in the model with three of their atoms, the α-carbon and two hydrogens along the backbone, held fixed from the X-ray structure in the geometry optimizations. The ligands that directly bind to the manganese atoms are Asp170, Glu189, His332, Glu333, Asp342, Ala344, and Glu354. These ligands were included in the previous studies

of the same type,[8,9] where the second shell charged ligand Arg357 was also included. The main difference in the present study is that Gln165, His337, and Asp61 were included as well. Since the manganese atoms are coordinated to each other by $\mu$-oxo bonds, only one water-derived ligand (a hydroxide) had to be added to the manganese outside the cube to fill up the full coordinations of all the manganese atoms. For calcium, two water ligands were added as ligands and one hydroxide connecting it to the manganese outside the cube. Finally, the same second shell water as in the previous studies was added, hydrogen bonded to one oxo ligand of the cube and to Arg357. The nomenclature for the S-states used in the discussion below is the same as that in previous studies. $S_n^m$ means that $n$ is the number of the S-state and $m$ is the charge of the complex (only including direct ligands to the OEC).

## III. S-State Transitions and O—O Bond Formation

Water oxidation in PSII proceeds in a sequence of four S-transitions from $S_0$ to $S_4$, in which the oxygen-evolving complex (OEC) is oxidized four times. Parallel to these oxidations, two substrate water molecules are deprotonated. At the final $S_4$-state, the O—O bond is formed and $O_2$ is released. To understand water oxidation therefore means understanding all the S-state transitions involved and finally the mechanism for the O—O bond formation. Ideally, the starting point for the calculations would have been a high-resolution X-ray structure for at least one of these S-states. Since the only available X-ray structures have rather low resolution of 3.0—3.5 Å and the structures furthermore could be affected by X-ray damage,[21] other approaches to this problem are needed. The approach and the results of the most recent investigations[8,9] will first be summarized before the new results are presented.

The earliest attempts to model water oxidation all led to a situation where an oxygen radical precedes O—O bond formation. An important step toward a low-barrier mechanism for O—O bond formation was taken when essentially all possibilities to form the O—O bond with the oxygen radical were investigated for the best available $S_4$-state.[5] Rather surprisingly, the lowest barrier by far was found for a reaction between the oxygen radical and a bridging oxo-group. Until then, the lowest barrier found was always one where the oxygen radical is attacked by an outside water,[11] but the barrier for that mechanism was already known to be far too high. What was even more surprising in the new mechanism was a spin-requirement for a low barrier. This requirement means

that all spins on the four most directly interacting atoms have to be alternant. The two oxygens have to have opposite spins to form a bond, and the manganeses binding these atoms have to have opposite spins to the respective oxygens. The reasons for the requirements on the manganese spins are in one case a formation of the reduced Mn(III) in a high-spin state and in the other case to allow O—O bond formation without crossing to another spin-surface.

Even though a rather clear picture of the O—O bond formation started to emerge, the connection of this mechanism to structural findings by X-ray and EXAFS techniques was relatively weak. Until then, rather crude models of the structure roughly following the X-ray suggestions had been used. To improve this situation, models were designed that followed the X-ray structures as closely as possible.[8] Since the X-ray structures have rather low resolution, the strategy to proceed is not obvious. One approach used has been to build a model of the entire enzyme and use a QM/MM technique to optimize the structure.[22] Still, an assumption of the general structure had to be made, and the strategy employed was to search for a minimum close to the London structure including the ligand pattern assumed in that structure. The results obtained from the QM/MM calculations have later been shown to match, besides the X-ray density, also results from polarized EXAFS experiments,[23] when the structure is allowed to distort slightly.[24] However, the available experimental information is probably not well enough defined to permit ruling out other structures. In the present approach, another strategy has been employed, by requiring that the structure should allow the low-barrier O—O bond formation in the $S_4$-state described above. With this starting point, a cluster model was built as described in section II and shown in Figure 2. By addition of electrons and protons to the $S_4$-state, structures for the lower S-states were eventually reached that could be compared with available experiments.[8] The following main conclusions were drawn. First, the structure obtained matches the London X-ray density very well. Second, a short Mn—Mn distance to the outer manganese was obtained, with two $\mu$-oxo bonds, in line with EXAFS interpretations[14,15] but in disagreement with the X-ray structures and the QM/MM structure. Third, a reconstruction of the OEC was found in the $S_2$ to $S_3$ transition, also in agreement with suggestions from EXAFS.[14,15] This reconstruction is caused by a binding of a water molecule, which opens up the OEC from the rather compact structure found for the lower S-states.

A mechanism for water oxidation has thus been achieved that both has a low barrier for O—O bond formation and is in basic structural agreement with experiments. However, fur-

ther computational model investigations complicated the picture. The main problem was that a new structure was found for the S$_2$-state that is 6 kcal/mol lower in energy than the previous one. The origin of the improved energy is a bidentate binding of Ala344 between a manganese and calcium, which in turn causes a rather big displacement of 0.8 Å for the hydroxyl group bridging between calcium and the outside manganese. The metal atoms do not move significantly. The corresponding change of the S$_3$-state did not lead to any improvement in energy. Since the S$_3$-state was already concluded to be too high in energy compared with the S$_2$-state by at least 3 kcal/mol in the previous study, the finding of the new S$_2$-state implies that an S$_3$-state has to be found nearly 10 kcal/mol lower in energy than before. A discrepancy of 3 kcal/mol is a tolerable difference using the present approach, but 10 kcal/mol is too much.

Improvements of the present results can be obtained in two ways. First, the models can be extended. Provided that the calculations are correct, which becomes more and more difficult for larger systems,[1] and that the same method is used, a larger model should be superior to a smaller one. However, the most recent extensions of the model have shown that the results are quite stable with respect to the size of the model. The second way to improve the results is to find a structure, within the same model, that is lower in energy. If a structure more than 5 kcal/mol lower in energy is found, the earlier one can be ruled out. In this way, gradually better structures with time can be guaranteed. Still, it can never be guaranteed that an even better structure does not exist that is lower in energy than the one found. However, with time and continued investigations, the likelihood of finding better structures will decrease. Convergence of the results can, of course, also be judged by comparisons to experiments.

There are two primary differences between the S$_2$ and S$_3$ states. First, the final manganese is oxidized in S$_3$ from Mn(III) to Mn(IV). Second, the reconstruction mentioned above occurs in this transition, caused by the binding of the second substrate water. After a large number of investigations improving both, these points finally led to a better S$_3$-state.

The first point addressed to improve the S$_3$-state was to investigate possibilities for other reconstructions in the S$_2$ to S$_3$ transition. The reconstruction found in the previous study[8] is given at the top in Figure 3. A water molecule (H$_2$O$_b$) first binds to the outer manganese (Mn4) and simultaneously loses a proton to the bulk. Since this manganese was already six-coordinated, the binding between Mn4 and O$_a$ is lost. O$_a$ instead binds to Mn2, which was originally five-coordinated with oxidation state III but is oxidized to Mn(IV) in this transi-
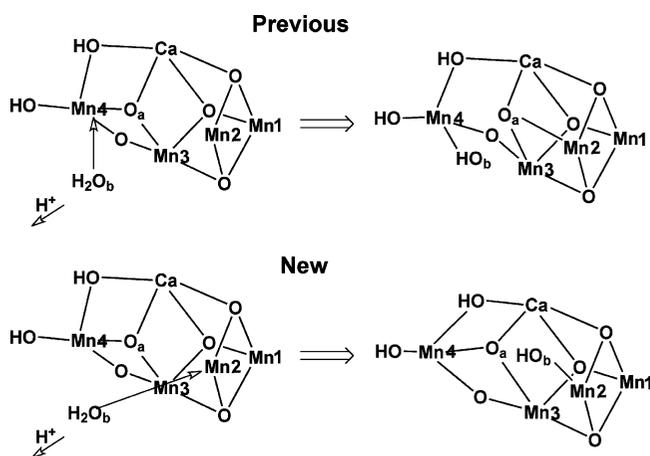


**FIGURE 3.** The previous and the new mechanism for water insertion, leading to the reconstruction in the S$_2$ to S$_3$ transition.

tion and therefore needs to become six-coordinated. In order to find an alternative to this process, attempts were made to directly bind the outside water to Mn2. Even though the structure is somewhat crowded it turns out that this is indeed possible if, again, a proton is lost from the water to the bulk in the binding process. A possible energetic advantage in the new scheme is that the reconstruction is significantly smaller than in the previous scheme. The largest effect is that Mn2 moves by 0.4 Å going from S$_2^{-1}$ to S$_2^{-2}$ (for nomenclature, see section II). The other metal atoms move less than 0.2 Å. The reason for this distortion is partly a crowding as water is added but also a change of direction of the Jahn−Teller axis on Mn2 in the Mn(III) oxidation state. The axis changes from pointing toward the empty site on Mn2 to pointing toward His332. The size of the new reconstruction can be compared with the much larger one in the previous scheme, where the outer manganese moves 1.4 Å and calcium 1.0 Å.

Even though the new reconstruction in Figure 3 appears to be less demanding than the previous one, there is quite surprisingly no energy advantage to it compared with the previous one.[9] On the contrary, it gave a higher energy of the S$_3$ state by 3 kcal/mol. However, an improvement was achieved if the new reconstruction was combined with another new effect. This effect was obtained when the second point addressed above, the one concerned with the ease of oxidation of Mn2, was studied. A very tedious investigation was performed, where quite different structures were considered (see below) including radical states, structures with chloride and bicarbonate, etc., but no improvement of the energy for the S$_3$-state was obtained. Finally, a major effect was found. It turned out that the exact ligation of Glu189 is very important for Mn2 oxidation. In the original positioning, Glu189 was bridging between Mn2 and calcium. By releasing the Glu189
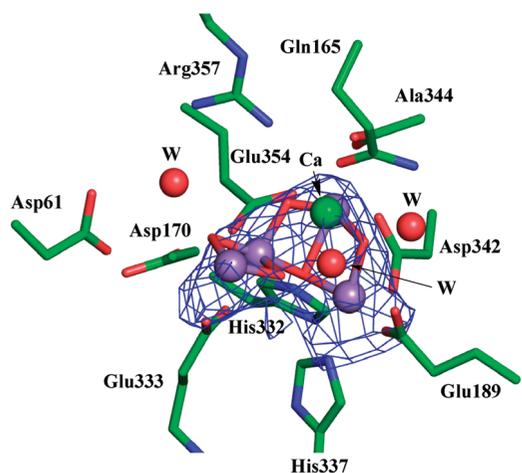
**FIGURE 4.** The DFT optimized $S_1^{-2}$-structure placed into the X-ray density from the Berlin X-ray measurements.

bond to calcium, and instead forming a hydrogen bond to a water molecule added on calcium, more of the negative charge on Glu189 is moved closer to Mn2, making it easier to oxidize. Even though it could have been expected that this might lead to an improvement, the size of the effect was much larger than expected, about 13 kcal/mol. After that finding, the energy of the $S_3$-state is now in the range it should be.

Before the detailed discussion of the S-state transitions, a few comments about the new structures should be made. First, the new structure of the $S_1$-state also fits the density from the X-ray experiments quite well. However, for the comparison to the density from the Berlin experiments, see Figure 4, it can be noted that the outer manganese is closer to the $Mn_3Ca$ cluster than the corresponding density is. A short bond to the outer manganese, as obtained here, is instead in agreement with interpretations of EXAFS experiments.[14,15] It can be suggested that the longer distance obtained in the Berlin X-ray study could be due to X-ray reduction,[21] which should have the largest effect on this distance. The Mn−Mn distances with three short (2.7−2.8 Å) and one long (3.2 Å) distance are also in good agreement with EXAFS interpretations. Even though the positions of the present structure fit the density of the Berlin structure reasonably well, there are rather large differences in the metal positions obtained, see Figure 5. The metal positions differ by between 0.5 and 1.4 Å.

In the search for a better $S_3$-state described above, many quite different structures were investigated. Some of these were the ones suggested by polarized EXAFS results.[23] In particular, attempts to find structures close to the IIa-structure were made. The metal atoms were first frozen in the relative positions suggested by EXAFS. It was not possible to fill all the coordinations of the metals in those positions if the backbone positions were taken from the X-ray studies. A few water

molecules therefore had to be added, as in the London structure. When the metal positions in IIa were released, there was a substantial energy improvement. Still, the energy was even after relaxation far worse than the one obtained for the best structures described above. The conclusion is that the metal positions in the IIa-structure are not consistent with the backbone positions obtained in the X-ray studies nor with the electron density of the OEC complex.

One consequence of the new reconstruction in Figure 3 is that the mechanism for O−O bond formation has to be slightly modified. When the proton is removed in the $S_3$ to $S_4$ transition from $HO_b$ in the structure at the bottom right in the figure, the oxygen radical will be formed on $O_b$ bound to Mn2. In the previous mechanism, the oxygen radical was bound to Mn4. However, a very similar O−O bond formation mechanism as before is obtained, see Figure 6. In the new mechanism, the $O_b$ radical will react with the oxo-group $O_a$, which means that the transition state structure will be very similar and the barrier as well. A difference is that now Mn4 will be reduced to Mn(III) as the O−O bond is formed, instead of Mn2 as before. The spin requirements are also very similar. If the $O_b$ radical has down-spin ($\beta$), it will form a bond with the $O_a$-oxo atom with up-spin ($\alpha$). The manganese being reduced, Mn4 in this case, must then have its d-electrons with down-spin, while the manganese (Mn2) initially holding the oxygen radical should have up-spin.

Another new aspect of the present mechanism is a different $S_3^{-2}$-state than before. This state has a Mn2(IV)=O bond, with a spin on oxygen that is quite high, +0.40. This state is almost as low in energy as the $S_3^{-1}$-state, where there is a Mn2(IV)−OH bond, with the usual low-spin population on oxygen of 0.04. The interesting aspect of these results is that the nature of the $S_2$ to $S_3$ transition has been strongly debated. Most experiments seem to indicate a manganese-centered oxidation,[25] while some EXAFS experiments have been interpreted as a ligand-centered oxidation.[26] Even though a Mn2(IV)=O state in $S_3$ should still formally be interpreted as a manganese oxidation, the high spin on oxygen could be taken as a sign of a strongly delocalized oxidation. Since the $S_3^{-1}$- and $S_3^{-2}$-states are so close in energy, it could depend on the conditions of the experiments which state is observed.

The S-transitions obtained from the present model (see section II) are shown schematically in Figure 7. The structures are taken from the optimizations but with all amino acids removed from the figure for clarity. The starting point, $S_0'$, is a state where O₂ has just been removed in the previous cycle. When O₂ is removed, there is a relatively large opening in the middle of the OEC where the first water substrate can be
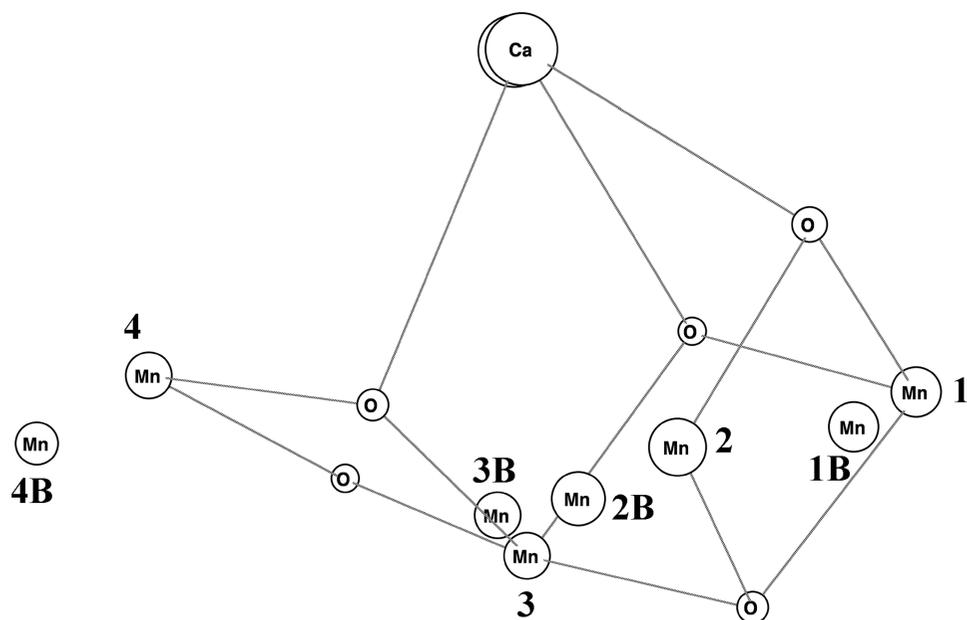
**FIGURE 5.** DFT structure superimposed on the Berlin X-ray structure. The X-ray atoms are marked with a B. The DFT atoms are connected with a thin line.
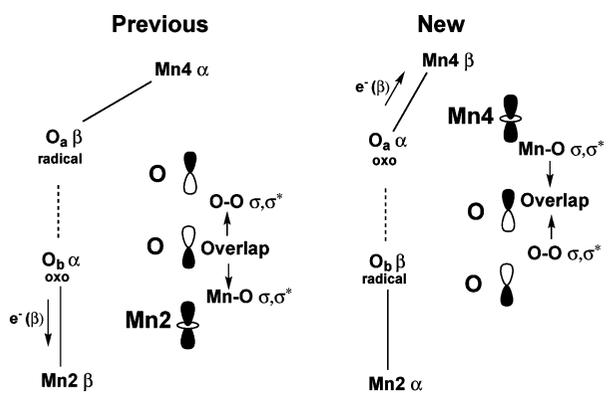


**FIGURE 6.** Schematic drawing of the previous and the new low-barrier mechanism for O−O bond formation discussed in the text. $\alpha$ and $\beta$ denote spin directions.

bound. It binds with a simultaneous loss of a proton to the bulk. The product is shown as $S_0$, where an arrow indicates the position of the substrate OH. In the $S_0$ to $S_1$ transition, an electron is removed from Mn4 (an ∗ marks the oxidation in $S_1$) and a proton is released to the bulk. The proton is taken from the substrate OH. In the $S_1$ to $S_2$ transition, only an electron is removed in agreement with experiments.[27−29] The electron is taken from Mn1. In the $S_2$ to $S_3$ transition, the next substrate water binds leading to the reconstruction illustrated at the bottom of Figure 3. The reconstruction occurs partly because there is not quite enough space for this water. A proton is simultaneously removed from the substrate water, exactly as in the formation of $S_0$, and an electron is taken from Mn2. In the $S_3$-state, all manganese are Mn(IV). In the final transition from $S_3$ to $S_4$, a proton is taken from the substrate OH and an electron from the substrate oxygen. Finally, the O−O bond is
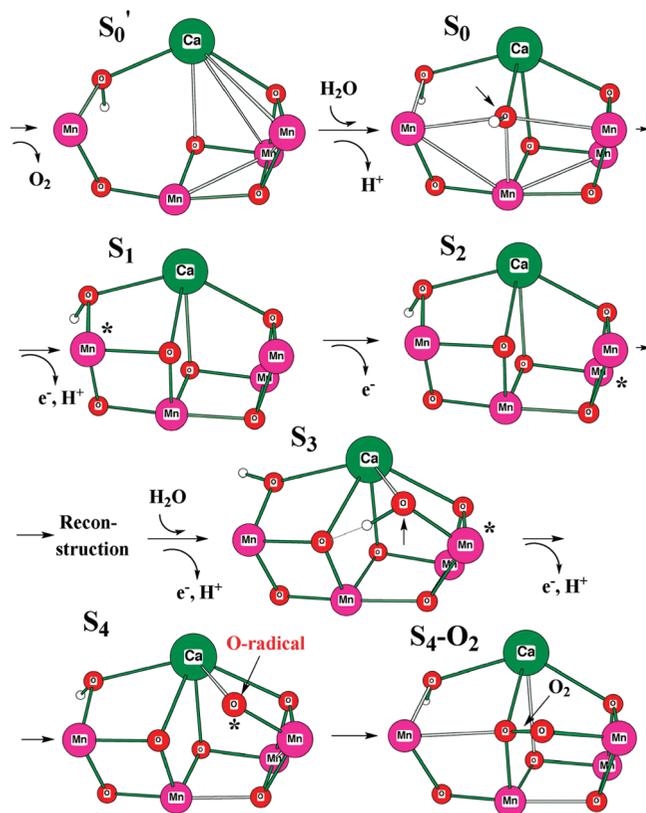


**FIGURE 7.** Schematic picture of the different S-transitions. The structures have been optimized, but only the most important atoms are shown. An ∗ marks the atom that has been oxidized in that transition.

formed between the oxygen radical and the oxo-group remaining from the first substrate water (see Figure 6), $O_2$ is released, and the cycle starts all over again. The structures

kcal/mol

— **Without membrane potential:**
barrier 10.7 kcal/mol

······· **With membrane potential:**
barrier 18.2 kcal/mol

$S_0^{-2}$ —0

$e^-$

$S_1^{-1}$ —7.2

$H^+$

—14.1

$S_1^{-2}$ —18.2

—20

$e^-$

—26.2

$S_2^{-1}$ —30.3

$H^+$ —28.9

$H_2O$ —20.7

—22.8

$S_2^{-2}$

$S_3^{-1}$ —31.0

$e^-$ —30.2

$H^+$

$S_3^{-2}$

—17.9

$S_4^{-1}$

—25.8

$e^-$

—13.5

O-O TS —8.0

—20.3

—40

$S_4^{-1}$
$O_2^{2-}$ —17.7

—25.1

$S_0^{-1}$

$S_4^{-1}$

$H_2O$

$O_2$ —30.0
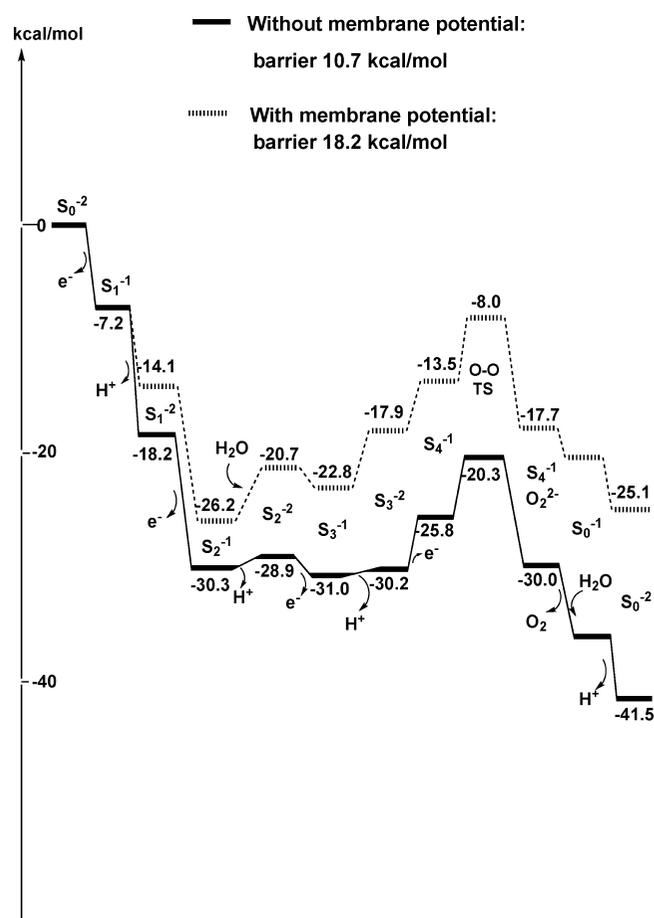
$S_0^{-2}$ —25.1

$H^+$ —41.5

**FIGURE 8.** Energy diagrams for dioxygen formation in PSII, with and without membrane gradient. The charge of the OEC alternates between −1 and −2.

show that the OEC forms a basin where the two substrate waters can naturally fit and be deprotonated, without much occurring in the rest of the complex.

With the calculated energies from the structures described above, it is possible to set up an energy diagram for the entire water oxidation process. To do this, the methods described in section II for obtaining p$K_a$ and redox potentials are used. The resulting diagrams are shown in Figure 8, both in the absence and in the presence of a membrane pH gradient. The pH gradient is taken to be 3 pH units, implying an additional cost of 4.1 kcal/mol for every proton that is released to the lumenal side. The driving force for the catalytic cycle is obtained as 41.5 kcal/mol, by using the redox potential for P$_{680}^+$ of 1.25 V[30,31] and for oxygen of 0.80 V. The value of 41.5 kcal/mol is slightly different from that used before, where the oxidation of Tyr$_Z$ was included as a an additional cost. The oxidation of Tyr$_Z$ is here instead discussed separately. Three more comments should be given before the energies are discussed. First, the positionings of the backbone atoms for Asp170 are at present quite uncertain from the X-ray studies. This resi-

due was therefore left without the backbone constraints in the most critical stage as the O−O bond is formed. Second, a spin-correction of −2.8 kcal/mol was added for the S$_4$-state structures. This correction was obtained from using a Heisenberg spin-Hamiltonian formalism[32] for the S$_4^{-1}$ oxygen radical state. Third, the hydrogen bonding for Asp61 is lost for the final peroxide state. This means that this residue will instead bind to something outside the model. A H-binding energy of −4.2 kcal/mol, the same as that found for Asp61 at the TS, is therefore added to the energy of the S$_4^{-1}$-O$_2$ state.

A general comment can first be made about the diagrams, and this is that the protons and electrons are removed in an alternating fashion. This has been the case also in all the previous investigations where energy diagrams were given; see, for example, ref 13. This preserves the charge of the catalyst as much as possible, which has been found to be an energetic advantage in enzyme mechanisms in general.[4] More recently, the model with alternating removal of charges has been used experimentally to analyze water oxidation in PSII and has been found to explain a large body of experimental results.[33]

The energy diagram without membrane potential in Figure 8 is similar in shape to the one obtained previously[8] but differs in detail. The first two S-transitions are quite exergonic. The third one from S$_2$ to S$_3$ was previously endergonic by 3.3 kcal/mol but is now slightly exergonic by 0.7 kcal/mol. The reasons for this change have been described in detail above. The formation of the oxygen radical in S$_4$ is endergonic as before but now by only 5.2 kcal/mol, compared with 11.9 kcal/mol before. The local O−O formation barrier is 5.5 kcal/mol compared with 6.5 kcal/mol before. This means that the total barrier for O−O bond formation is now 10.7 kcal/mol, substantially lower than the one before of 18.4 kcal/mol. The new barrier is therefore consistent with a process that takes milliseconds. The transition from S$_3$ to S$_0$ was previously found to be only slightly exergonic by 3.7 kcal/mol but is now exergonic by 11.3 kcal/mol. This means that the present values are no longer consistent with the experimental suggestion of a reversible O−O bond cleavage from S$_0$.[34]

Three additional amino acids were included in the present model compared with the previous one, Gln165, His337, and Asp61. To find an optimal position for Gln165 turned out to be quite difficult. By adding another water on calcium, the best position for Gln165 was finally found with a binding directly to calcium. This was the case for all S-states except S$_0$ where a position further out from calcium was found optimal. After the positioning of Gln165 was determined, the difference of having this ligand in the model compared with just having a

water on calcium, as in the previous study, is almost negligible. The energy diagrams look essentially the same. In contrast, the optimal position for His337 with a hydrogen bond to one of the oxo groups was very easy to find, and this position does not change in the S-transitions. Since the charge of the OEC cluster varies between $-2$ and $-1$, attempts were made to put another proton on the histidine, but the energy was very poor. His337 has an interesting effect on the S-transitions. The ionization potentials (related to redox potentials) of Mn2 and Mn3 are increased by about 5 kcal/mol, but there is no effect on Mn1 or the oxygen that becomes the oxygen radical. Therefore, even though only relative energies are used to construct the energy diagram, His337 will have a non-negligible energetic effect on the S-transitions. This effect is partly compensated by a corresponding, but smaller, effect on the proton affinities ($pK_a$ values). Finally, Asp61 was added since it is generally believed to be part of the proton transfer pathway. The calculations show that this residue is protonated. This can to some extent be understood by the negative charge on the OEC, but it is surprising that it is significantly better energetically to protonate Asp61 than His337. The energetic effects on the diagram of adding Asp61 are very small. With the protonation states found, the entire model will vary between a charge of 0 and $-1$, with the OEC itself varying between $-1$ and $-2$.

The barrier obtained for the case with a membrane gradient is 18.2 kcal/mol (with respect to the $S_2$-state), which is somewhat too large compared with what can be expected from experiments. However, with respect to the $S_3$ state, the barrier is only 14.8 kcal/mol. The low energy for the $S_2$ state must be regarded as an error, since this state should not be lower than the $S_3$-state even with a membrane gradient. The error of a few kcal/mol is tolerable with respect to errors that have to be expected with the present methods. However, this error could also be an indication of a minor remaining problem with the chemical model used. For example, as noted above, the positioning of Asp170 is uncertain, and further investigations are needed to safely position this residue. An interesting aspect of the energy diagrams is that as much as 25 kcal/mol is wasted as heat for every $O_2$ molecule produced even with a maximal gradient. This is more than half of the energy available after the charge separation in the reaction center. The reason so much energy is lost is, of course, to increase the rate of the process.

Tyr$_Z$ oxidation is an intermediate step in the oxidation of the OEC by $P_{680}^+$. So far in the analysis, this step has not been considered, partly because Tyr$_Z$ is outside the chemical model used. However, by simple electrostatic arguments, approxi-
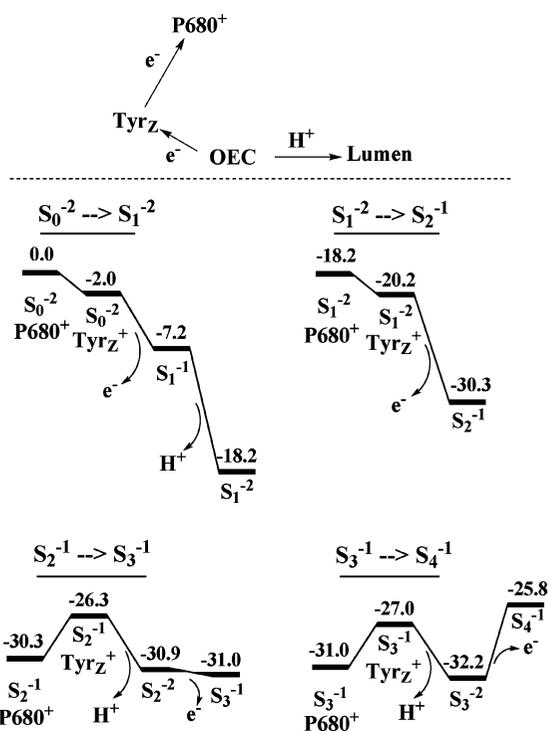


**FIGURE 9.** Energy diagrams for the different S-transitions, including Tyr$_Z$ oxidation.

mate diagrams can be drawn including Tyr$_Z$ oxidation in the different S-transitions, see Figure 9. These diagrams were constructed with two assumptions. First, the electrostatic effect of a charge on His190 (a proton) has to be estimated. The distances from the $\epsilon$-nitrogen on His190 and the Mn-atoms are in the range 8−9 Å. With a dielectric constant of 4, as used in previous studies, this would lead to an average effect of about 9 kcal/mol. This is considered as a too large effect, and in the present study, $\epsilon = 6$ was therefore used instead, which leads to an effect of about 6 kcal/mol on the OEC. The effect on the diagrams in Figure 8 is negligible by this change, since only relative values are used in their construction. A second assumption has to be made on the energy loss, when Tyr$_Z$ is oxidized by $P_{680}^+$ in the $S_1$ to $S_2$ transition. Since oxidized Tyr$_Z$ is observed as an intermediate in this transition, its redox potential has to be smaller than the one of $P_{680}^+$. The assumption is that 2 kcal/mol is lost in this transition. This leads to an estimated redox potential for Tyr$_Z$ of 1.16 V in $S_1$.

With the above two assumptions, the diagrams for the first two transitions in Figure 9 are easily constructed. The same energies as in the diagrams in Figure 8 are used. The results for the third and fourth transition are more interesting. Since only an electron is released in the $S_1$ to $S_2$ transition, there is a proton remaining on the OEC in $S_2$ at the stage when Tyr$_Z$ is oxidized. With a repulsive effect from this proton, the oxidation of Tyr$_Z$ will now be uphill by 4 kcal/mol, instead of

downhill by 2 kcal/mol as in the previous transitions. It is important to note that, unlike the earlier transitions, there will not be any loss of energy as $Tyr_Z$ is oxidized. With the presence of the plus charge on $Tyr_Z^+$, it will be easier to remove a proton from the OEC. Instead of an uphill process of 1.4 kcal/mol, as in the diagram in Figure 8, there is now a downhill process of 4.6 kcal/mol (a difference of 6.0 kcal/mol, as assumed). To reach the same $S_3^{-1}$-level as in Figure 8, the electron removal from OEC becomes exergonic by 0.1 kcal/mol. The diagram for the next transition is constructed similarly. It can be noted that the diagrams are consistent with the experimental observation that the OEC becomes deprotonated as $Tyr_Z$ is oxidized in the $S_3$ to $S_4$ transition.[35] They are also consistent with fast $Tyr_Z$ oxidations in $S_0$ to $S_1$ and $S_1$ to $S_2$ and with a slow, proton-coupled $S_2$ to $S_3$ transition.[36]

The details of proton transfer within the model shown in Figure 2 have recently been described, as well as oxygen release.[37] The suggested pathway for proton release in the $S_1$ to $S_2$ transition involves key roles of an outside water and the motion of Asp170. An electron transfer between manganese centra during the proton release was also found to be important. For releasing dioxygen in the $S_4$-state, entropy plays a major role.

## IV. Summary

Recent hybrid DFT calculations using models with up to 170 atoms have confirmed but also slightly modified previous findings for the mechanism of water oxidation in PSII. The best O—O bond formation mechanism found remains one with a reaction between an oxygen radical and a $\mu$-oxo ligand, but the oxygen radical is now found to bind to a different manganese center. A previously found reconstruction in the $S_2$ to $S_3$ transition is energetically improved by binding the water molecule to a manganese in the $Mn_3Ca$-cube instead of to the outer manganese. A model for substrate water binding has also been described where the OEC forms a basin where the two substrate waters can naturally fit and be deprotonated, see Figure 7. The new calculations lead to improved energy diagrams in comparison to experiments.

*I am very grateful to Dr James Murray for making Figure 4.*

## BIOGRAPHICAL INFORMATION

**Per E. M. Siegbahn** received his Ph.D. degree at Stockholm University in 1973 and has been on its staff as Professor since 1983. His interests have varied over the years from development of ab initio quantum chemical methods to the application to gas-phase reactions of small molecules, to models of homogeneous and het-

erogeneous catalysis, and to his present main interest in mechanisms of redox-active enzymes.

## REFERENCES

1 Siegbahn, P. E. M.; Himo, F. Recent Developments of the Quantum Chemical Cluster Approach for Modeling Enzyme Reactions. *J. Biol. Inorg. Chem.* **2009**, *39*, 2923–2935.

2 Ferreira, K. N.; Iverson, T. M.; Maghlaoui, K.; Barber, J.; Iwata, S. Architecture of the Photosynthetic Oxygen Evolving Center. *Science* **2004**, *303*, 1831–1838.

3 Loll, B.; Kern, J.; Saenger, W.; Zouni, A.; Biesiadka, J. Towards Complete Cofactor Arrangement in the 3.0 Å Resolution Structure of Photosystem II. *Nature* **2005**, *438*, 1040–1044.

4 Siegbahn, P. E. M.; Blomberg, M. R. A. Modeling of Mechanisms for Metalloenzymes Where Protons and Electrons Enter or Leave. In *Computational Modeling for Homogeneous Catalysis and Biocatalysis*; Morokuma, K., Musaev, J., Eds.; Wiley-VCH: Weinheim, Germany, 2008; pp 57–81.

5 Siegbahn, P. E. M. O-O Bond Formation in the $S_4$-State of the Oxygen Evolving Complex in Photosystem II. *Chem.—Eur. J.* **2006**, *12*, 9217–9227.

6 Siegbahn, P. E. M. Mechanism and Energy Diagram for O-O Bond Formation in the Oxygen Evolving Complex in Photosystem II. *Proc. R. Soc.* **2008**, *363*, 1221–1228.

7 Siegbahn, P. E. M. Theoretical Studies of O-O Bond Formation in Photosystem II. *Inorg. Chem.* **2008**, *47*, 1779–1786.

8 Siegbahn, P. E. M. A Structure Consistent Mechanism for Dioxygen Formation in Photosystem II. *Chem.—Eur. J.* **2008**, *27*, 8290–8302.

9 Siegbahn, P. E. M. Water Oxidation by the Manganese Cluster in Photosynthesis. In *Computational Inorganic and Bioinorganic Chemistry*; Solomon, E. I., King, B., Scott, R., Eds.; John Wiley and Sons, Ltd: Chichester, England, 2009.

10 Siegbahn, P. E. M.; Blomberg, M. R. A. The Combined Picture from Theory and Experiments on Water Oxidation, Oxygen Reduction and Proton Pumping. *J. Chem. Soc., Dalton Trans.* **2009**, 5832–5840.

11 Siegbahn, P. E. M.; Crabtree, R. H. Manganese Oxyl Radical Intermediates and O-O Bond Formation in Photosynthetic Oxygen Evolution and a Proposed Role for the Calcium Cofactor in Photosystem II. *J. Am. Chem. Soc.* **1999**, *121*, 117–127.

12 Siegbahn, P. E. M. Theoretical Models for the Oxygen Radical Mechanism of Water Oxidation and of the Water Oxidizing Complex of Photosystem II. *Inorg. Chem.* **2000**, *39*, 2923–2935.

13 Siegbahn, P. E. M.; Lundberg, M. The Mechanism for Dioxygen Formation in PSII Studied by Quantum Chemical Methods. *Photochem. Photobiol. Sci.* **2005**, *4*, 1035–1043.

14 Liang, W.; Roelofs, T. A.; Cinco, R. M.; Rompel, A.; Latimer, M. J.; Yu, W. O.; Sauer, K.; Klein, M. P.; Yachandra, V. K. Structural Change of the Mn Cluster During the $S_2$ to $S_3$ State Transition of the Oxygen-Evolving Complex of Photosystem II. Does it Reflect the Onset of Water/Substrate Oxidation? Determination by Mn X-ray Absorption Spectroscopy. *J. Am. Chem. Soc.* **2000**, *122*, 3399–3412.

15 Haumann, M.; Muller, C.; Liebisch, P.; Iuzzolino, L.; Dittmer, J.; Grabolle, M.; Neisius, T.; Meyer-Klaucke, W.; Dau, H. Structural and Oxidation State Changes of the Photosystem II Manganese Complex in Four Transitions of the Water Oxidation Cycle ($S_0$ to $S_1$, $S_1$ to $S_2$, $S_2$ to $S_3$, and $S_3$, $S_4$ to $S_0$,) Characterized by X-ray Absorption Spectroscopy at 20 K and Room Temperature. *Biochemistry* **2005**, *44*, 1894–1908.

16 Becke, A. D. Density-Functional Thermochemistry. 3. The Role of Exact Exchange. *J. Chem. Phys.* **1993**, *98*, 5648–5652.

17 Reiher, M.; Salomon, O.; Hess, B. A. Reparameterization of Hybrid Functinals Based on Energy Differences of States of Different Multiplicity. *Theor. Chem. Acc.* **2001**, *107*, 48–55.

18 Siegbahn, P. E. M. The Performance of Hybrid DFT on Mechanisms Involving Transition Metal Complexes in Enzymes. *J. Biol. Inorg. Chem.* **2006**, *11*, 695–701.

19 Jaguar 5.5, Schrödinger, L. L. C., Portland, OR (1991–2003).

20 Frisch, M. J.; Trucks, G. W.; Schlegel, H. B.; Scuseria, G. E.; Robb, M. A.; Cheeseman, J. R.; Montgomery, J. A., Jr.; Vreven, T.; Kudin, K. N.; Burant, J. C.; Millam, J. M.; Iyengar, S. S.; Tomasi, J.; Barone, V.; Mennucci, B.; Cossi, M.; Scalmani, G.; Rega, N.; Petersson, G. A.; Nakatsuji, H.; Hada, M.; Ehara, M.; Toyota, K.; Fukuda, R.; Hasegawa, J.; Ishida, M.; Nakajima, T.; Honda, Y.; Kitao, O.; Nakai, H.; Klene, M.; Li, X.; Knox, J. E.; Hratchian, H. P.; Cross, J. B.; Bakken, V.; Adamo, C.; Jaramillo, J.; Gomperts, R.; Stratmann, R. E.; Yazyev, O.; Austin, A. J.; Cammi, R.; Pomelli, C.; Ochterski, J. W.; Ayala, P. Y.; Morokuma, K.; Voth, G. A.; Salvador, P.; Dannenberg, J. J.; Zakrzewski, V. G.; Dapprich, S.; Daniels, A. D.; Strain, M. C.; Farkas, O.; Malick, D. K.; Rabuck, A. D.; Raghavachari, K.; Foresman, J. B.; Ortiz, J. V.; Cui, Q.; Baboul, A. G.; Clifford, S.; Cioslowski, J.; Stefanov, B. B.; Liu, G.; Liashenko, A.; Piskorz, P.; Komaromi, I.; Martin, R. L.; Fox, D. J.; Keith, T.; Al-Laham, M. A.; Peng, C. Y.; Nanayakkara, A.; Challacombe, M.; Gill, P. M. W.;

Johnson, B.; Chen, W.; Wong, M. W.; Gonzalez, C.; Pople, J. A. *Gaussian 03*, revision B.03; Gaussian Inc., Pittsburg, PA, 2003.

21  Yano, J.; Kern, J.; Irrgang, K.-D.; Latimer, M. J.; Bergmann, U.; Glatzel, P.; Pushkar, Y.; Biesiadka, J.; Loll, B.; Sauer, K.; Messinger, J.; Zouni, A.; Yachandra, V. K. X-ray Damage to the $Mn_4$ Ca Complex in Single Crystals of Photosystem II: A Case Study for Metalloprotein Crystallography. *Proc. Natl. Acad. Sci. U.S.A.* **2005**, *102*, 12047–12052.

22  Sproviero, E. M.; Gascon, J. A.; McEvoy, J. P.; Brudvig, G. W.; Batista, V. S. QM/MM Models of the $O_2$-Evolving Complex of Photosystem II. *J. Chem. Theor. Comput.* **2006**, *4*, 1119–1134. Sproviero, E. M.; Gascon, J. A.; McEvoy, J. P.; Brudvig, G. W.; Batista, V. S. Structural Models of the Oxygen-Evolving Complex of Photosystem II. *Curr. Opin. Struct. Biol.* **2007**, *17*, 173–180. Sproviero, E. M.; Shinopoulos, K.; Gascon, J. A.; McEvoy, J. P.; Brudvig, G. W.; Batista, V. S. QM/MM Computational Studies of Substrate Water Binding to the Oxygen Evolving Complex of Photosystem II. *Philos. Trans. R. Soc. B* **2008**, *363*, 1149–1156. Sproviero, E. M.; Gascon, J. A.; McEvoy, J. P.; Brudvig, G. W.; Batista, V. S. Qunatum Mechanics/Molecular Mechanics Study of the Catalytic Cycle of Water Splitting in Photosystem II. *J. Am. Chem. Soc.* **2008**, *130*, 3428–3442.

23  Yano, J.; Kern, J.; Sauer, K.; Latimer, M. J.; Pushkar, Y.; Biesiadka, J.; Loll, B.; Saenger, W.; Messinger, J.; Zouni, A.; Yachandra, V. K. Where Water is Oxidized to Dioxygen: Structure of the Photosynthetic $Mn_4$ Ca Cluster. *Science* **2006**, *314*, 821–825.

24  Sproviero, E. M.; Gascon, J. A.; McEvoy, J. P.; Brudvig, G. W.; Batista, V. S. A Model of the Oxygen-Evolving Center of Photosystem II Predicted by Structural Refinement Based on EXAFS Simulations. *J. Am. Chem. Soc.* **2008**, *130*, 6728–6730.

25  Iuzzolino, L.; Dittmer, J.; Dörner, W.; Meyer-Klaucke, W.; Dau, H. X-Ray Absorption Spectroscopy on Layered Photosystem II Membrane Particles Suggests Manganese Centered Oxidation of the Oxygen-Evolving Complex for the $S_0$ to $S_1$, $S_1$ to $S_2$, and $S_2$ to $S_3$ Transitions of the Water Oxidation Cycle. *Biochemistry* **1998**, *37*, 17112–17119.

26  Messinger, J.; Robblee, J. H.; Bergmann, U.; Fernandez, C.; Glatzel, P.; Visser, H.; Cinco, R. M.; McFarlane, K. L.; Bellacchio, E.; Pizarro, S. A.; Cramer, S. P.; Sauer, K.; Klein, M. P.; Yachandra, V. K. Absence of Mn-Centered Oxidation in the $S_2$ to $S_3$

Transition: Implications for the Mechanism of Photosynthetic Water Oxidation. *J. Am. Chem. Soc.* **2001**, *123*, 7804–7820.

27  Fowler, C. F. Proton Evolution From Photosystem II. Stoichiometry and Mechanistic Considerations. *Biochim. Biophys. Acta* **1997**, *462*, 414–421.

28  Saphon, S.; Crofts, A. R. Protolytic Reactions in Photosystem II: A New Model for the Release of Protons Accompanying the Photooxidation of Water. *Z. Naturforsch.* **1977**, *32C*, 617–626.

29  Förster, V.; Junge, W. Stoichiometry and Kinetics of Proton Release upon Photosynthetic Water Oxidation. *Photochem. Photobiol.* **1985**, *41*, 183–190.

30  Diner, B. A. Amino Acid Residues Involved in the Coordination and Assembly of the Manganese Cluster of Photosystem II. Proton-Coupled Electron Transport of the Redox-Active Tyrosines and its Relationship to Water Oxidation. *Biochim. Biophys. Acta* **2001**, *1503*, 147–163.

31  Rappaport, F.; Lavergne, J. Coupling of Electron and Proton Transfer in the Photosynthetic Water Oxidase. *Biochim. Biophys. Acta* **2001**, *1503*, 246–259.

32  Noodleman, L.; Case, D. A. Density-Functional Theory of Spin Polarization and Spin Coupling in Iron-Sulfur Clusters. *Adv. Inorg. Chem.* **1992**, *38*, 423–470.

33  Dau, H.; Haumann, M. Eight Steps Preceding O-O Bond Formation in Oxygenic Photosynthesis - A Basic Reaction Cycle of the Photosystem II Manganese Complex. *Biochim. Biophys. Acta* **2007**, *1767*, 472–483.

34  Clausen, J.; Junge, W. Detection of an Intermediate of Photosynthetic Water Oxidation. *Nature* **2004**, *430*, 480–483.

35  Haumann, M.; Liebisch, P.; Müller, C.; Barra, M.; Grabolle, M.; Dau, H. Photosynthetic $O_2$ Formation Tracked by Time-Resolved X-ray Experiments. *Science* **2005**, *310*, 1019–1021.

36  Hillier, W.; Messinger, J. Mechanism of Photosynthetic Oxygen Production. In *Photosystem II. The Light-Driven Water: Plastoquinone Oxidoreductase*; Wydrzynski, T. Satoh, K., Eds.; Advances in Photosynthesis and Respiration; Springer: Dordrecht, The Netherlands, 2005; Vol. 22, 567.

37  Siegbahn, P. E. M. Water Oxidation in Photosystem II: Oxygen Release, Proton Release and the Effect of Chloride. *Dalton Trans.* **2009**, DOI: 10.1039/b909470a.